Momentum and energy distributions of nucleons in finite nuclei due to short-range correlations

H. Müther
Institut für Theoretische Physik, Universität Tübingen, Auf der Morgenstelle 14, D-72076 Tübingen, Germany

A. Polls
Departament d'Estructura i Constituens de la Materia, Universitad de Barcelona, Diagonal 647, E-08028 Barcelona, Spain

W.H. Dickhoff
Department of Physics, Washington University, St. Louis, Missouri 63130
(Received 8 November 1994)

The influence of short-range correlations on the momentum and energy distribution of nucleons in nuclei is evaluated assuming a realistic meson-exchange potential for the nucleon-nucleon interaction. Using the Green-function approach the calculations are performed directly for the finite nucleus ^{16}O avoiding the local density approximation and its reference to studies of infinite nuclear matter. The nucleon-nucleon correlations induced by the short-range and tensor components of the interaction yield an enhancement of the momentum distribution at high momenta as compared to the Hartree-Fock description. These high-momentum components should be observed mainly in nucleon knockout reactions like $(e, e'p)$ leaving the final nucleus in a state of high excitation energy. Our analysis also demonstrates that non-negligible contributions to the momentum distribution should be found in partial waves which are unoccupied in the simple shell model. The treatment of correlations beyond the Brueckner-Hartree-Fock approximation also yields an improvement for the calculated ground-state properties.

PACS number(s): 21.10.Jx, 21.30.+y, 24.10.Cn, 27.20.+n

I. INTRODUCTION

Many properties of nuclei can be understood within the independent particle model (IPM). In the IPM the nucleus is considered to be a system of nucleons moving without residual interaction in a mean field or single-particle potential. The single-particle potential is either adjusted in a phenomenological way (assuming, e.g., a Woods-Saxon shape) or evaluated from empirical effective interactions like the Skyrme forces within the Hartree-Fock approximation. Attempts to employ realistic nucleon-nucleon (NN) interactions, which reproduce the NN scattering data, directly in such a scheme fail badly: Typically one does not even obtain any binding energy in this approach. This result is due to the strong short-range and tensor components, which are typical for realistic interactions and induce corresponding NN correlations in the nuclear wave function, which cannot be described by the IPM or the Hartree-Fock approach.

Various tools have been developed to account for these strong short-range correlations. These include variational calculations assuming Jastrow correlation functions [1], the correlated basis function method (CBF) [2], the "exponential S" method [3], the Brueckner-Hartree-Fock (BHF) approximation [4], and the self-consistent Green-function approach [5].

Considerable effort has also been made to find a nuclear property which is experimentally accessible and reflects the effects of NN correlations in a clear manner. A candidate for such an observable is the momentum distribution of nucleons in a nucleus. Of course the momentum distribution is a single-particle observable and thus allows only an indirect measurement of correlation effects. In particular the uncertainties in the determination of an optimal one-body Hamiltonian lead to uncertainties in the analysis of the momentum distribution with respect to correlation effects. Nevertheless, a careful analysis of the momentum distribution may give some indications of the importance of correlation effects. This momentum distribution can be written as

$$n(k) = \sum_{l,j,\tau} (2j+1)\, n_{lj\tau}(k) = \sum_{l,j,\tau} (2j+1)\, \langle \Psi_0^A | \, a_{klj\tau}^\dagger a_{klj\tau} \, | \Psi_0^A \rangle \,. \quad (1)$$

Here $|\Psi_0^A\rangle$ represents the ground state of the nucleus under consideration (with A nucleons) and $a_{klj\tau}^\dagger$ ($a_{klj\tau}$) denotes the creation (annihilation) operator for a nucleon with orbital angular momentum l, total angular momentum j, isospin τ, and momentum k. The momentum distributions for the partial waves, $n_{lj\tau}(k)$, in Eq. (1) can be rewritten by inserting a complete set of eigenstates $|\Psi_n^{A-1}\rangle$ for the system with $A-1$ nucleons,

$$n_{lj\tau}(k) = \sum_n |\langle \Psi_n^{A-1} | \, a_{klj\tau} \, | \Psi_0^A \rangle|^2 . \quad (2)$$

In the IPM the sum in this equation is typically reduced to one term, if (l, j, τ) refer to a single-particle orbit occu-

 ©1995 The American Physical Society

pied in $|\Psi_0^A\rangle$. Equation (2) then yields the square of the momentum-space wave function for this single-particle state. The contribution $n_{lj\tau}(k)$ vanishes in the IPM if no state with quantum numbers (l, j, τ) is occupied. If correlations are present beyond the IPM approach this simple picture is no longer true and the determination of the momentum distribution $n(k)$ requires, both in experimental as well as theoretical studies, complete knowledge of the nucleon-hole spectral function

$$S_{lj\tau}(k,E) = \sum_n |\langle \Psi_n^{A-1}| a_{klj\tau} |\Psi_0^A\rangle|^2 \times \delta(E - (E_0^A - E_n^{A-1})) \quad (3)$$

for all energies E and all sets of discrete quantum numbers (l, j, τ). Note that the energy variable E in this definition of the spectral function refers to the negative excitation energy of state n in the $A-1$ system with respect to the ground-state energy of the nucleus with A nucleons (E_0^A). The spectral function is experimentally accessible by analyzing nucleon knockout experiments like $(e, e'p)$. The momentum distribution $n_{lj\tau}(k)$ is obtained by integrating the spectral function over energies E from $-\infty$ to the Fermi energy $\epsilon_F = E_0^A - E_0^{A-1}$, with E_0^{A-1} denoting the energy of the ground state for $A-1$ nucleons. One important aim of our studies is to investigate how short-range correlations modify the spectral function at various energies as compared to the IPM. For example, can one expect to observe effects of short-range correlations in knockout experiments with small energy transfer?

Microscopic calculations of the spectral function and the momentum distribution based on realistic nuclear Hamiltonians have mainly been performed for very light nuclei ($A \leq 4$) [6–9] or nuclear matter [10–17]. Results for heavier nuclei are typically derived from investigations of nuclear matter assuming a local density approximation [18–21]. Recent variational calculations for ^{16}O yield the momentum distribution [22] and the p-shell quasihole wave functions [23] but not the complete energy dependence of the hole spectral functions.

The present investigation determines the spectral function and the corresponding momentum distribution directly for finite nuclei without employing the local density approximation. Calculations are performed for the nucleus ^{16}O assuming a realistic meson-exchange potential [24] for the NN interaction. The spectral function is derived from the Lehmann representation of the single-particle Green function. This Green function solves the Dyson equation with a self-energy calculated by techniques as described in Ref. [25]. In this approach the self-energy is evaluated in terms of a nuclear matter G matrix considering all terms up to second order in this G matrix (see Fig. 1). The calculation of the self-energy itself is performed for the finite nucleus employing a mixed basis of single-particle states with oscillator functions for the internal hole states and plane waves, properly orthogonalized to the hole states, for the intermediate particle states occurring in the diagrams of Fig. 1. Using this mixed representation one can obtain more reliable results for the momentum distribution at high momenta than can be deduced from BHF of finite nuclei for which typically all single-particle states are described by an expansion in an oscillator basis [26]. A few results concerning the spectral function for the $p_{1/2}$ partial wave have already been discussed [27].

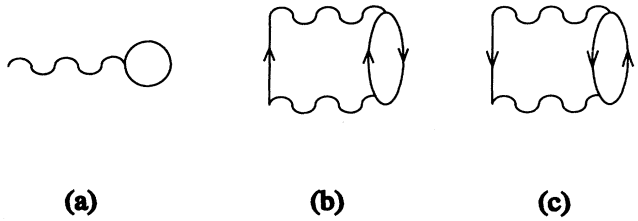

FIG. 1. Graphical representation of the Hartree-Fock (a), the two-particle–one-hole [2p1h, (b)] and the two-hole–one-particle contribution [2h1p, (c)] to the self-energy of the nucleon.

Special attention is paid to the effect of correlations on the spectral function at different energies. We find that clear indications of the short-range NN correlations are obtained by studying the spectral function at very negative energies, which in nucleon knockout experiments correspond to excitation energies of around 100 MeV and more in the remaining nucleus. The resulting Green function is also used to study the effects of correlations beyond the BHF approach on the binding energy and radius of the nuclear ground state.

After this short Introduction we describe the techniques used to evaluate the spectral functions and momentum distributions in Sec. II. The results of our numerical studies are presented in Sec. III and Sec. IV summarizes the main conclusions of this work.

II. EVALUATION OF THE SPECTRAL FUNCTIONS

The spectral function for the various partial waves, $S_{lj\tau}(k,E)$ [see Eq. (3)], can be obtained from the imaginary part of the corresponding single-particle Green function or propagator $g_{lj}(k,k;E)$. Note that here and in the following we have dropped the isospin quantum number τ. Ignoring the Coulomb interaction between the protons the Green functions are identical for $N = Z$ nuclei and therefore independent of the quantum number τ. The single-particle propagator can be obtained by solving the Dyson equation

$$g_{lj}(k_1,k_2;E) = g_{lj}^{(0)}(k_1,k_2;E) + \int dk_3 \int dk_4 g_{lj}^{(0)}(k_1,k_3;E)\Delta\Sigma_{lj}(k_3,k_4;E)g_{lj}(k_4,k_2;E), \quad (4)$$

where $g^{(0)}$ refers to a Hartree-Fock propagator and $\Delta\Sigma_{lj}$ represents contributions to the real and imaginary parts of the irreducible self-energy, which go beyond the Hartree-Fock approximation of the nucleon self-energy used to derive $g^{(0)}$. The definition and evaluation of the Hartree-Fock contribution as well as the calculation of $\Delta\Sigma$ are presented in the next subsection. The methods used to solve the Dyson equation (4) and to extract spectral functions as well as momentum distributions are described in Sec. II B.

A. Nucleon self-energy Σ

The calculation of the self-energy is performed in terms of a G matrix which is obtained as a solution of the Bethe-Goldstone equation for nuclear matter

$$\begin{aligned}\langle k'l'SJ_SKLT|\,G\,|k''l''SJ_SKLT\rangle &= \langle k'l'SJ_SKLT|\,V_{NN}\,|k''l''SJ_SKLT\rangle \\ &+\sum_l \int k^2dk\ \langle k'l'SJ_SKLT|\,V_{NN}\,|klSJ_SKLT\rangle \\ &\times \langle klSJ_SKLT|\,G\,|k''l''SJ_SKLT\rangle\ \frac{Q(k,K)}{\omega_{\rm NM}-\frac{K^2}{4m}-\frac{k^2}{2m}}\,. \end{aligned} \tag{5}$$

In this equation k, k', and k'' denote the relative momentum, l, l', and l'' the orbital angular momentum for the relative motion, K and L are the corresponding quantum numbers for the center-of-mass motion, S and T denote the total spin and isospin of the interacting pair of nucleons, and by definition the angular momentum J_S is obtained from coupling the orbital angular momentum of relative motion and the spin S. For the bare NN interaction V_{NN} we have chosen the one-boson-exchange (OBE) potential B defined by Machleidt ([24], Table A.2), m represents the mass of the nucleon, and the Pauli operator Q is approximated by the so-called angle-averaged approximation for nuclear matter with a Fermi momentum $k_F = 1.4$ fm^{-1}. This roughly corresponds to the saturation density of nuclear matter. The starting energy $\omega_{\rm NM}$ has been chosen to be -10 MeV. The choices for the density of nuclear matter and the starting energy are rather arbitrary. It turns out, however, that the calculation of the Hartree-Fock term is not very sensitive to this choice [28]. Furthermore, we will correct this nuclear matter approximation by calculating the two-particle–one-hole (2p1h) term displayed in Fig. 1(b) directly for the finite system, correcting the double counting contained in the Hartree-Fock term (see discussion below).

Using vector bracket transformation coefficients [29], the G-matrix elements obtained from (5) can be transformed from the representation in coordinates of relative and center-of-mass momenta to the coordinates of single-particle momenta in the laboratory frame in which the two-particle state would be described by quantum numbers such as

$$|k_1l_1j_1k_2l_2j_2JT\rangle\,, \tag{6}$$

where k_i, l_i, and j_i refer to momentum and angular momenta of particle i whereas J and T define the total angular momentum and isospin of the two-particle state. It should be noted that Eq. (6) represents an antisymmetrized two-particle state. Performing an integration over one of the k_i, one obtains a two-particle state in a mixed representation of one particle in a bound harmonic oscillator while the other is in a plane wave state,

$$\begin{aligned}&|n_1l_1j_1k_2l_2j_2JT\rangle \\ &\quad=\int_0^\infty dk_1\,k_1^2R_{n_1,l_1}(\alpha k_1)\ |k_1l_1j_1k_2l_2j_2JT\rangle\,. \end{aligned} \tag{7}$$

Here R_{n_1,l_1} stands for the radial oscillator function and the oscillator length $\alpha = 1.72$ fm^{-1} has been selected. This choice for the oscillator length corresponds to an oscillator energy of $\hbar\omega_{\rm osc} = 14$ MeV. Therefore the oscillator functions are quite appropriate to describe the wave functions of the bound single-particle states in ^{16}O. Indeed, it turns out that the single-particle wave functions determined in self-consistent BHF calculations for ^{16}O have a large overlap with these oscillator functions [26]. Using the nomenclature defined in Eqs. (5)–(7) our Hartree-Fock approximation for the self-energy is easily obtained in the momentum representation,

$$\Sigma^{\rm HF}_{l_1j_1}(k_1,k_1') = \frac{1}{2(2j_1+1)}\sum_{n_2l_2j_2JT}(2J+1)(2T+1)\,\langle k_1l_1j_1n_2l_2j_2JT|\,G\,|k_1'l_1j_1n_2l_2j_2JT\rangle\,. \tag{8}$$

The summation over the oscillator quantum numbers is restricted to the states occupied in the IPM of ^{16}O. This Hartree-Fock part of the self-energy is real and does not depend on the energy.

The terms of lowest order in G which give rise to an imaginary part in the self-energy are represented by the diagrams displayed in Figs. 1(b) and 1(c), referring to intermediate 2p1h and two-hole–one-particle (2h1p) states, respectively. The 2p1h contribution to the imaginary part is given by

$$W^{2p1h}_{l_1j_1}(k_1,k_1';E) = \frac{-1}{2(2j_1+1)} \sum_{n_2l_2j_2} \sum_{lL} \sum_{JJ_SST} \int k^2dk \int K^2dK(2J+1)(2T+1)$$
$$\times \langle k_1 l_1 j_1 n_2 l_2 j_2 JT| G |klSJ_SKLT\rangle \langle klSJ_SKLT| G |k_1' l_1 j_1 n_2 l_2 j_2 JT\rangle$$
$$\times \pi\delta\left(E + \epsilon_{n_2l_2j_2} - \frac{K^2}{4m} - \frac{k^2}{m}\right), \tag{9}$$

where the "experimental" single-particle energies $\epsilon_{n_2l_2j_2}$ are used for the hole states (−47 MeV, −21.8 MeV, and −15.7 MeV for $s_{1/2}$, $p_{3/2}$, and $p_{1/2}$ states, respectively), while the energies of the particle states are given in terms of the kinetic energy only. The expression in Eq. (9) still ignores the requirement that the intermediate particle states must be orthogonal to the hole states, which are occupied for the nucleus under consideration. The techniques to incorporate the orthogonalization of the intermediate plane wave states to the occupied hole states as discussed in detail by Borromeo *et al.* [25] have also been used here. The 2h1p contribution to the imaginary part $W^{2h1p}_{l_1j_1}(k_1,k_1';E)$ can be calculated in a similar way (see also [25]).

Our choice to assume pure kinetic energies for the particle states in calculating the imaginary parts of W^{2p1h} [Eq. (9)] and W^{2h1p} may not be very realistic for the excitation modes at low energy. Indeed a sizable imaginary part in W^{2h1p} is obtained only for energies E below −40 MeV. As we are mainly interested, however, in the effects of short-range correlations, which lead to excitations of particle states with high momentum, the choice seems to be appropriate. A different approach would be required to treat the coupling to the very low-lying two-particle–one-hole and two-hole–one-particle states in an adequate way. Attempts at such a treatment can be found in Refs. [30–33].

The 2p1h contribution to the real part of the self-energy can be calculated from the imaginary part W^{2p1h} using a dispersion relation [34]

$$V^{2p1h}_{l_1j_1}(k_1,k_1';E) = \frac{P}{\pi} \int_{-\infty}^{\infty} \frac{W^{2p1h}_{l_1j_1}(k_1,k_1';E')}{E'-E} dE', \tag{10}$$

where P means a principal value integral. From the δ function in Eq. (9) one can see that W^{2p1h} is different from zero only for positive values of E'. Since the diagonal matrix elements are negative, the dispersion relation (10) implies that the diagonal elements of V^{2p1h} will be attractive for negative energies E. They will decrease and change sign only for large positive values for the energy of the interacting nucleon (typically around a few hundred MeV, depending on the interaction used).

Since the Hartree-Fock contribution Σ^{HF} has been calculated in terms of a nuclear matter G matrix, it already contains 2p1h terms of the kind displayed in Fig. 1(b). Therefore one would run into problems of double counting if one simply adds the real part V^{2p1h} to the Hartree-Fock self-energy. Notice that Σ^{HF} does not contain any imaginary part because it is calculated with a nuclear matter G matrix at a starting energy for which G is real. In order to avoid such an overcounting of the particle-particle ladder terms, we subtract from the real part of the self-energy a correction term, which just contains this contribution calculated in nuclear matter. This correction V_c is given by

$$V_c(k_1,k_1') = \frac{1}{4(2j_1+1)} \sum_{n_2l_2j_2} \sum_{lL} \sum_{JJ_SST} \int k^2dk \int K^2dK(2J+1)(2T+1)$$
$$\times \langle k_1 l_1 j_1 n_2 l_2 j_2 JT| G |klSJKLT\rangle \langle klSJKLT| G |k_1' l_1 j_1 n_2 l_2 j_2 JT\rangle \frac{Q(k,K)}{\omega_{NM} - \frac{K^2}{4m} - \frac{k^2}{m}}, \tag{11}$$

with the same starting energy ω_{NM} and the Pauli operator Q as used in the Bethe-Goldstone equation (5).

A dispersion relation similar to Eq. (10) holds for V^{2h1p} and W^{2h1p},

$$V^{2h1p}_{l_1j_1}(k_1,k_1';E) = -\frac{P}{\pi} \int_{-\infty}^{\infty} \frac{W^{2h1p}_{l_1j_1}(k_1,k_1';E')}{E'-E} dE'. \tag{12}$$

Since W^{2h1p} is positive (at least its diagonal matrix elements) and different from zero for negative energies E' only, it is evident from Eq. (12) that V^{2p1h} is repulsive for positive energies and decreases with increasing energy. Only for large negative energies does it becomes attractive.

Summing up the various contributions we obtain for the self-energy the expressions

$$\Sigma = \Sigma^{HF} + \Delta\Sigma$$
$$= \Sigma^{HF} + \left(V^{2p1h} - V_c + V^{2h1p}\right) + i\left(W^{2p1h} + W^{2h1p}\right). \tag{13}$$

B. Solution of the Dyson equation

After we have determined the various contributions to the nucleon self-energy, we now want to solve the Dyson equation (4) for the single-particle propagator. In order to discretize the integrals in this equation we consider a complete basis within a spherical box of a radius R_{box}. This box radius should be larger than the radius of the nucleus considered. The calculated observables are independent of the choice of R_{box}, if it is chosen to be around

15 fm or larger. A complete and orthonormal set of regular basis functions within this box is given by

$$\Phi_{iljm}(\mathbf{r}) = \langle \mathbf{r}|k_i ljm\rangle = N_{il} j_l(k_i r)\mathcal{Y}_{ljm}(\theta\phi) \ . \quad (14)$$

In this equation $\mathcal{Y}_{ljm}$ represent the spherical harmonics including the spin degrees of freedom and j_l denote the spherical Bessel functions for the discrete momenta k_i which fulfill

$$j_l(k_i R_{\rm box}) = 0. \quad (15)$$

Using the normalization constants

$$N_{il} = \begin{cases} \frac{\sqrt{2}}{\sqrt{R^3_{\rm box}} j_{l-1}(k_i R_{\rm box})} & \text{for } l > 0, \\ \frac{i\pi\sqrt{2}}{\sqrt{R^3_{\rm box}}} & \text{for } l = 0, \end{cases} \quad (16)$$

the basis functions defined in Eq. (14) are orthogonal and normalized within the box,

$$\int_0^{R_{\rm box}} d^3r \ \langle k_{i'} l' j' m'|\mathbf{r}\rangle \langle \mathbf{r}|k_i ljm\rangle = \delta_{ii'}\delta_{ll'}\delta_{jj'}\delta_{mm'}. \quad (17)$$

Note that the basis functions defined for discrete values of the momentum k_i within the box differ from the plane wave states defined in the continuum with the corresponding momentum just by the normalization constant, which is $\sqrt{2/\pi}$ for the latter. This enables us to determine the matrix elements of the nucleon self-energy in the basis of Eq. (14) from the results presented in the preceding section.

As a first step we determine the Hartree-Fock approximation for the single-particle Green function in the "box basis." For that purpose the Hartree-Fock Hamiltonian is diagonalized,

$$\sum_{n=1}^{N_{\rm max}} \langle k_i| \frac{k_i^2}{2m}\delta_{in} + \Sigma^{\rm HF}_{lj} |k_n\rangle \langle k_n|\alpha\rangle_{lj} = \epsilon^{\rm HF}_{\alpha lj} \langle k_i|\alpha\rangle_{lj} \ . \quad (18)$$

Here and in the following the set of basis states in the box has been truncated by assuming an appropriate $N_{\rm max}$. In the basis of Hartree-Fock states $|\alpha\rangle$, the Hartree-Fock propagator is diagonal and given by

$$g^{(0)}_{lj}(\alpha; E) = \frac{1}{E - \epsilon^{\rm HF}_{\alpha lj} \pm i\eta}, \quad (19)$$

where the sign in front of the infinitesimal imaginary quantity $i\eta$ is positive (negative) if $\epsilon^{\rm HF}_{\alpha lj}$ is above (below) the Fermi energy. With these ingredients one can solve the Dyson equation (4). One possibility is to determine first the so-called reducible self-energy, originating from an iteration of $\Delta\Sigma$, by solving

$$\langle\alpha|\, \Sigma^{\rm red}_{lj}(E)\, |\beta\rangle = \langle\alpha|\, \Delta\Sigma_{lj}(E)\, |\beta\rangle + \sum_\gamma \langle\alpha|\, \Delta\Sigma_{lj}(E)\, |\gamma\rangle \times g^{(0)}_{lj}(\gamma; E) \langle\gamma|\, \Sigma^{\rm red}_{lj}(E)\, |\beta\rangle \quad (20)$$

and obtain the propagator from

$$g_{lj}(\alpha, \beta; E) = g^{(0)}_{lj}(\alpha; E) \langle\alpha|\, \Sigma^{\rm red}_{lj}(E)\, |\beta\rangle\, g^{(0)}_{lj}(\beta; E). \quad (21)$$

Using this representation of the Green function one can calculate the spectral function in the "box basis" from

$$\tilde{S}^c_{lj}(k_i, E) = \frac{1}{\pi}{\rm Im}\left(\sum_{\alpha,\beta} \langle k_i|\alpha\rangle_{lj}\, g_{lj}(\alpha, \beta; E)\, \langle\beta|k_i\rangle_{lj}\right). \quad (22)$$

For energies E below the lowest single-particle energy of a given Hartree-Fock state (with lj) this spectral function is different from zero only due to the imaginary part in $\Sigma^{\rm red}$. This contribution involves the coupling to the continuum of 2h1p states and is therefore nonvanishing only for energies at which the corresponding irreducible self-energy $\Delta\Sigma$ has a nonzero imaginary part. Besides this continuum contribution, the hole spectral function also receives contributions from the quasihole states [5]. The energies and wave functions of these quasihole states can be determined by diagonalizing the Hartree-Fock Hamiltonian plus $\Delta\Sigma$ in the "box basis,"

$$\sum_{n=1}^{N_{\rm max}} \langle k_i| \frac{k_i^2}{2m}\delta_{in} + \Sigma^{\rm HF}_{lj} + \Delta\Sigma_{lj}(E = \epsilon^{\rm qh}_{\Upsilon lj})\, |k_n\rangle \langle k_n|\Upsilon\rangle_{lj} = \epsilon^{\rm qh}_{\Upsilon lj} \langle k_i|\Upsilon\rangle_{lj} \ . \quad (23)$$

Since in the present work $\Delta\Sigma$ only contains a sizable imaginary part for energies E below $\epsilon^{\rm qh}_\Upsilon$, the energies of the quasihole states come out real and the continuum contribution to the spectral function is separated in energy from the quasihole contribution. The quasihole contribution to the hole spectral function is given by

$$\tilde{S}^{\rm qh}_{\Upsilon lj}(k_i, E) = Z_{\Upsilon lj} \left|\langle k_i|\Upsilon\rangle_{lj}\right|^2 \delta(E - \epsilon^{\rm qh}_{\Upsilon lj}), \quad (24)$$

with the spectroscopic factor for the quasihole state given by [5]

$$Z_{\Upsilon lj} = \left(1 - \frac{\partial \langle\Upsilon|\, \Delta\Sigma_{lj}(E)\, |\Upsilon\rangle}{\partial E}\bigg|_{\epsilon^{\rm qh}_{\Upsilon lj}}\right)^{-1}. \quad (25)$$

Finally, the continuum contibution of Eq. (22) and the quasihole parts of Eq. (24), which are obtained in the basis of box states, can be added and renormalized to obtain the spectral function in the continuum representation at the momenta defined by Eq. (15),

$$S_{lj}(k_i, E) = \frac{2}{\pi}\frac{1}{N_{il}^2}\left(\tilde{S}^c_{lj}(k_i, E) + \sum_\Upsilon \tilde{S}^{\rm qh}_{\Upsilon lj}(k_i, E)\right). \quad (26)$$

C. Ground-state properties

The single-particle propagator calculated by the techniques described above may also be used to evaluate expectation values of single-particle operators, like the mean square radius and the energy of the ground state. For that purpose one also needs the nondiagonal part of the density matrix, which is given in the "box basis," defined in the preceding subsection, by

$$\tilde{n}_{lj}(k_i,k_n) = \int_{-\infty}^{\epsilon_F} dE\, \frac{1}{\pi}\mathrm{Im} \times \left(\sum_{\alpha,\beta} \langle k_i|\alpha\rangle_{lj}\, g_{lj}(\alpha,\beta;E)\, \langle\beta|k_n\rangle_{lj} \right), \tag{27}$$

and contains, as before in the case of the spectral function, a continuous contribution and a part originating from the quasihole states,

$$\tilde{n}^{\mathrm{qh}}_{lj}(k_i,k_n) = \sum_{\Upsilon} Z_{\Upsilon lj}\, \langle k_i|\Upsilon\rangle_{lj}\, \langle\Upsilon|k_n\rangle_{lj}\,. \tag{28}$$

The sum in this equation is restricted to quasihole states with energies below the Fermi energy ϵ_F. With this density matrix the expectation value for the square of the radius can be calculated according to

$$\left\langle \Psi_0^A \right| r^2 \left| \Psi_0^A \right\rangle = \sum_{l,j} 2(2j+1) \sum_{i,n=1}^{N_{\max}} \langle k_i|\, r^2\, |k_n\rangle_l\, n_{lj}(k_i,k_n), \tag{29}$$

with a factor of 2 accounting for isospin degeneracy. The matrix elements for r^2 are given by

$$\langle k_i|\, r^2\, |k_n\rangle_l = N_{il} N_{nl} \int_0^{R_{\mathrm{box}}} dr\, r^4\, j_l(k_i r) j_l(k_n r)\,. \tag{30}$$

In the same way one can also calculate the expectation value for the particle number. The total energy of the ground state is obtained from the "Koltun sum rule"

$$E_0^A = \sum_{l,j} 2(2j+1) \sum_{i=1}^{N_{\max}} \int_{-\infty}^{\epsilon_F} dE\, \frac{1}{2}\left(\frac{k_i^2}{2m} + E\right) \times \left(\tilde{S}^c_{lj}(k_i,E) + \sum_{\Upsilon} \tilde{S}^{\mathrm{qh}}_{\Upsilon lj}(k_i,E) \right). \tag{31}$$

As in Eq. (26), the sum over quasihole states Υ is restricted to those below ϵ_F.

III. RESULTS AND DISCUSSION

In our discussion of the hole spectral function in the preceding section we have distinguished the contributions originating from the quasihole states and the continuum of 2h1p configurations [see Eq. (26)]. This separation can also be made when we discuss the momentum distributions for the various partial waves [see Eq. (2)], which are given as the energy-integrated spectral function (including all energies below the Fermi energy ϵ_F)

$$n_{lj}(k) = \int_{-\infty}^{\epsilon_F} dE\, \left[S^c_{lj}(k,E) + S^{\mathrm{qh}}_{lj}(k,E) \right]. \tag{32}$$

This separation into the two parts is displayed in Fig. 2 for various partial waves. This figure displays quite clearly that the momentum distribution at small momenta is dominated by the quasihole contribution (for those partial waves for which it exists) whereas the high-momentum components are given by the continuum part (see also Ref. [27]).

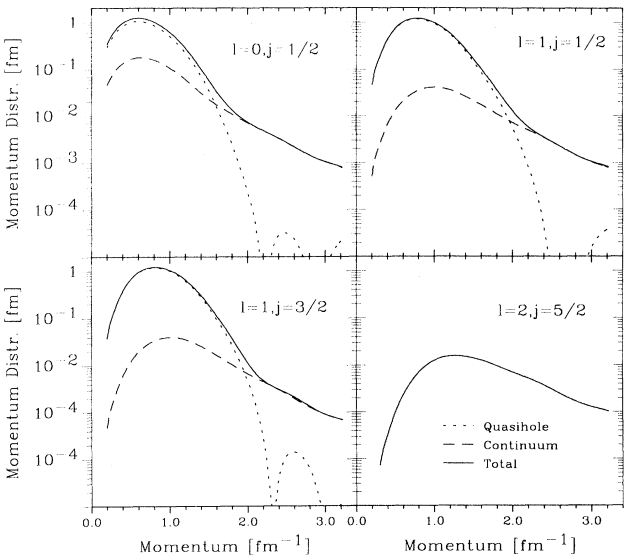

FIG. 2. Momentum distribution for different partial waves in ^{16}O [see Eq. (32)]. The momentum distribution is the sum of the quasihole contribution (dashed curve) and the continuum contribution (dotted curve). All functions are normalized such that $\int dk\, n(k) = 1$ if $S(k)$ refers to an orbit which is mostly occupied.

This implies that a nucleon knockout reaction with small energy transfer, leaving the remaining nucleus (e.g., ^{15}N in the present case as all results presented here refer to ^{16}O) in its ground state or in the lowest state with angular momentum and parity defined by the partial wave quantum numbers j and l, should display a spectral distribution as presented by the quasihole part. The high-momentum components of the spectral function (or momentum distribution) should only be observed in experiments which also include knockout processes into states represented by the 2h1p continuum. We recall that the present approach has been designed to account for the effects of short-range correlations. Effects due to configuration mixing of the hole state with the 2h1p configuration at low energies must be treated in terms of shell-model configuration mixing or by techniques as discussed in Refs. [30–33].

In order to characterize the energy dependence of the spectral functions one may define a mean value for the energy of the 2h1p continuum for each momentum and each partial wave by

$$\mathcal{E}_{lj}(k) = \frac{\int dE\, E\, S^c_{lj}(k,E)}{\int dE\, S^c_{lj}(k,E)}\,. \tag{33}$$

Typical values for this mean value range from -80 to -150 MeV for the momenta k considered in this analysis ($k \leq 3.3$ fm^{-1}). One also finds that this mean value is

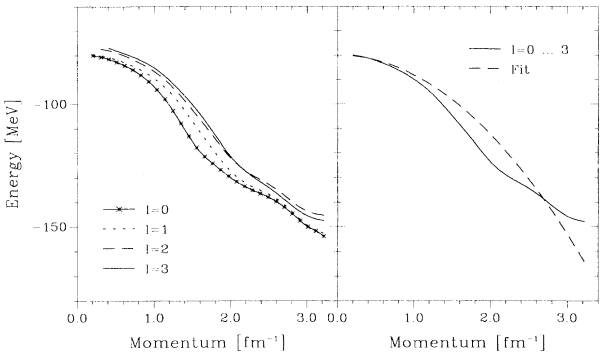

FIG. 3. Mean value for the energy of the 2h1p continuum as a function of the momentum k. The left part of this figure shows results for $\mathcal{E}_{lj}$ [see Eq. (33)] in various partial waves. In the right part of the figure the mean value averaged for the various l and j [see Eq. (34)] is displayed. For comparison this part also includes a simple parametrization in terms of $-k^2/(2m^*) - C$ with $m^* = 2400$ MeV and $C = 80$ MeV.

quite independent of the partial wave considered (see left part of Fig. 3). Therefore it is useful to define a mean value of the energy by averaging over all partial waves,

$$\mathcal{E}(k) = \frac{\sum_{l,j}(2j+1)\int dE\, E\, S^c_{lj}(k,E)}{\sum_{l,j}(2j+1)\int dE\, S^c_{lj}(k,E)} \,. \tag{34}$$

The resulting energy spectrum $\mathcal{E}(k)$ is shown in the left part of Fig. 3 and compared to a simple parametrization of this curve in terms of $-k^2/(2m^*) - C$ with $m^* = 2400$ MeV and $C = 80$ MeV. This parametrization demonstrates that the momentum dependence of this mean value is weak as compared, e.g., to the kinetic energy. One may also compare the mean value $\mathcal{E}(k)$ determined by Eq. (34) in ^{16}O with the corresponding quantity obtained for nuclear matter using the Reid potential [14,35]. The mean value calculated for nuclear matter shows a stronger momentum dependence and therefore, at high momenta, yields energies considerably below those displayed in Fig. 3. This implies that the nuclear matter calculation exhibits a larger probability to excite 2p1h configurations at higher energies as compared to the present approach. We will come back to a discussion of possible differences between the present calculation and studies in nuclear matter when we analyze the results for the momentum distribution below.

In order to show the importance of the continuum part of the spectral functions as compared to the quasihole contribution and to visualize the effects of correlations, we have included in Table I the particle numbers for each partial wave including the degeneracy of the states,

$$\hat{n}_{lj} = 2(2j+1)\int_{-\infty}^{\epsilon_F} dE \int_0^{\infty} dk\, k^2 S_{lj}(k,E) \,, \tag{35}$$

also separating the contributions originating from the quasihole states and those due to the continuum.

In the present approach the quasihole states, which in a Hartree-Fock approximation would be occupied with a probability of 1.0, are occupied with a probability of 0.78, 0.91, and 0.90 in the case of $s_{1/2}$, $p_{3/2}$, and $p_{1/2}$, respectively. This means that only 14.025 out of the 16 nucleons of ^{16}O occupy the quasihole states. Another 1.13 "nucleons" are found in the 2h1p continuum with partial wave quantum numbers of the s and p shells, while an additional 0.687 "nucleons" are obtained from the continuum with orbital quantum numbers of the d and f shells. The distinction between quasihole and continuum contributions is somewhat artificial for the $s_{1/2}$ orbital since the coupling to low-lying 2h1p states leads to a strong fragmentation of the strength [36], which is also observed experimentally [37]. A recent $(e,e'p)$ experiment on ^{16}O [38] has provided detailed information on the spectroscopic factors at low-energy transfer. The analysis of the experiment indicates that, e.g., the $p_{1/2}$ quasihole state carries only 63% of the strength. This result should be compared to the 90% obtained here. This

TABLE I. Distribution of nucleons in ^{16}O. Listed are the total occupation number $\hat{n}$ for various partial waves [see Eq. (35)] but also the contributions from the quasihole ($\hat{n}^{\rm qh}$) and the continuum part ($\hat{n}^{\rm c}$) of the spectral function, separately. The continuum part is split further into contributions originating from energies E below -150 MeV [$n^c(E<-150)$] and from energies below -100 MeV. The last line shows the sum of particle numbers for all partial waves listed.

lj	$\hat{n}^{\rm qh}$	$\hat{n}^c(E<-150)$	$\hat{n}^c(E<-100)$	$\hat{n}^c$	$\hat{n}$	$\hat{n}/[2(2j+1)]$
$s_{1/2}$	3.120	0.033	0.244	0.624	3.744	0.936
$p_{3/2}$	7.314	0.032	0.133	0.332	7.646	0.956
$p_{1/2}$	3.592	0.026	0.086	0.173	3.764	0.941
$d_{5/2}$	0.0	0.033	0.106	0.234	0.234	0.020
$d_{3/2}$	0.0	0.036	0.108	0.196	0.196	0.025
$f_{7/2}$	0.0	0.025	0.063	0.117	0.117	0.007
$f_{5/2}$	0.0	0.032	0.084	0.140	0.140	0.012
$\sum$	14.025	0.217	0.824	1.816	15.841	

discrepancy is partly due to the emphasis in the present work on the accurate treatment of short-range correlations. Long-range (low-energy) correlations, not considered in this work, typically yield another 10% reduction of the quasihole strength [30–33,36]. It has also been observed that a correct treatment of the center-of-mass motion may be responsible for another 10% reduction in the quasihole strength [23].

The sum of the particle numbers listed in Table I is slightly smaller (15.841) than the particle number corresponding to ^{16}O. There are several possible sources for this discrepancy: First of all our analysis only accounts for momenta k below 3.3 fm^{-1} and we did not consider partial waves with $l > 3$. The restriction in k is determined by the choice of $N_{\max}$ in truncating the "box basis" [see, e.g., Eq. (18)]. Inspecting the decrease of the occupation numbers listed in Table I with increasing l one can expect that the "missing" nucleons may be found in partial waves with $l > 3$. Furthermore, however, one must keep in mind that the present approach to the single-particle Green function is not number conserving, as the Green functions used to evaluate the self-energy are not determined in a self-consistent way [5]. It should be pointed out that the depletion of the occupation probabilities of the hole states, indicated in Table I, is particularly large for the $s_{1/2}$ orbit. This feature can be ascribed to the closeness of the $s_{1/2}$ Hartree-Fock energy to the 2h1p continuum which yields more leakage of strength to the continuum than for the $p_{1/2}$ and $p_{3/2}$ quasihole states.

Inspecting the contributions to $\hat{n}^c_{lj}$ originating from the various energy regions in Table I, one can see that the major contributions are obtained from energies around -100 MeV. Only small contributions come from energies below -150 MeV. The same feature is also obtained if one analyzes the momentum-integrated spectral function of the continuum,

$$N^c(E) = \sum_{l,j} 2(2j+1) \int_0^\infty dk\, k^2\, S^c_{lj}(k,E)\ , \qquad (36)$$

shown in Fig. 4. As a function of the energy of the 2h1p states, this density of states rises very rapidly just below our threshold for 2h1p configurations at ≈ -40 MeV, shows a maximum at -60 MeV and a second local maximum around -85 MeV, reflecting possibly some shell structure, and smoothly vanishes at lower energies. This density of states corresponds to a prediction of the total spectral strength to be observed in knockout reactions as a function of the energy transfer.

The contribution of the 2h1p continuum to the momentum distribution is presented in Fig. 5, exhibiting the contributions from partial waves with various l. The momentum distributions displayed in this figure contain the degeneracy factors $2(2j+1)$ and are normalized in such a way that $\int dk n_l(k)$ yields the total number of particles with orbital angular momentum l in the 2p1h continuum. This figure also shows that the largest contributions are obtained for $l = 0$, although the degeneracy factor is small in this case. One can see, however, that the decrease of the contributions with increasing l

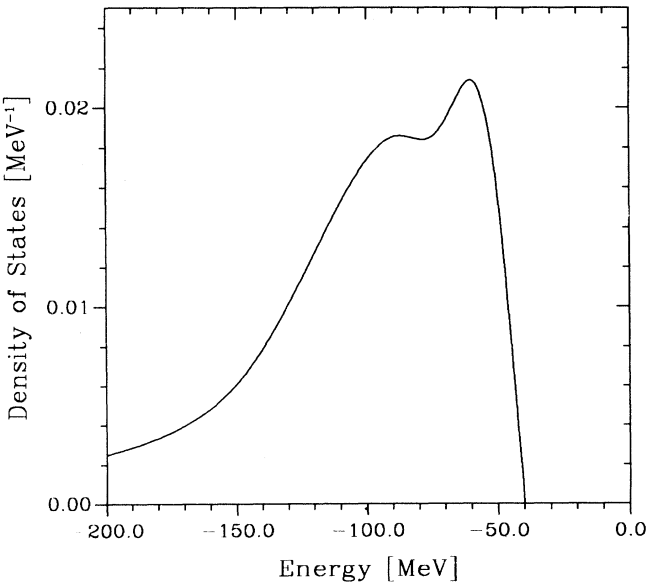

FIG. 4. Density of states or total occupation probability of the 2h1p continuum as a function of the energy E [see Eq. (36)]. The normalization of this distribution is such that the integration over the energy yields the total particle number of 1.816 (see Table I) in the continuum.

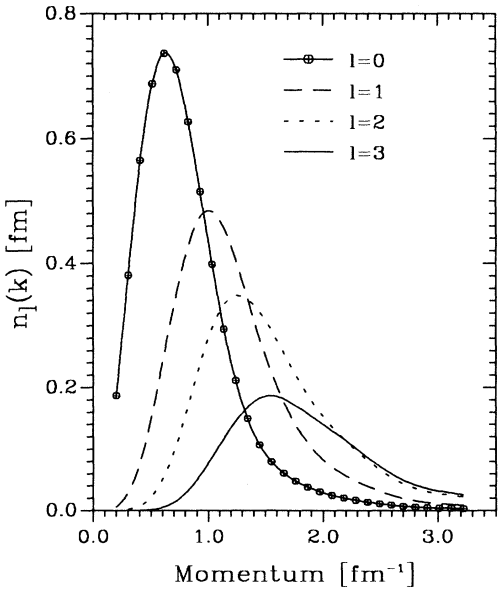

FIG. 5. The momentum distribution for various orbital angular momenta. These distribution account for the different j, include the degeneracy factors $2(2j+1)$, and are normalized in such a way that $\int dk n_l(k)$ yields the total number of particles with orbital angular momentum l in the 2p1h continuum.

is slow, supporting the above argument that the missing particle number exhibited in Table I should be obtained from partial waves with $l > 3$. In addition, the centroid of the momentum distribution is shifted to higher momenta with increasing l. At momenta $k \approx 3$ fm^{-1} the largest contribution is obtained from $l = 3$.

The total momentum distribution, including the contribution from the quasihole states, is shown in Fig. 6. This distribution is presented for various energy cutoffs. The quasihole part reflects the cross section for knockout reactions with small energy transfer, i.e., leading to the ground state of the final nucleus and excited states up to ≈ 20 MeV. The curve denoted by $E > -100$ MeV should reflect the momentum distribution including all states of the final nucleus up to around 80 MeV, etc. As has been discussed already in connection with the spectral functions of Fig. 2 (see also Ref. [27]), the high-momentum components of the momentum distribution due to short-range correlations are expected to be observable mainly in knockout experiments with an energy transfer of the order of 100 MeV.

The total momentum distributions resulting from the quasihole states and the 2h1p continuum are displayed again in Fig. 7 and compared to predictions from studies in nuclear matter [14,39]. In order to enable the comparison with the nuclear matter results, the momentum distributions resulting from the present studies have been divided by the particle number and are normalized in this figure such that $\int d^3k\, n(k)$ yields 1. In order to demonstrate the sensitivity of the calculated momentum distribution we show in this figure results obtained for the Reid soft-core potential as well as those evaluated from the OBE potential B, which is also used in our study of ^{16}O. The modern OBE potentials are considered to be

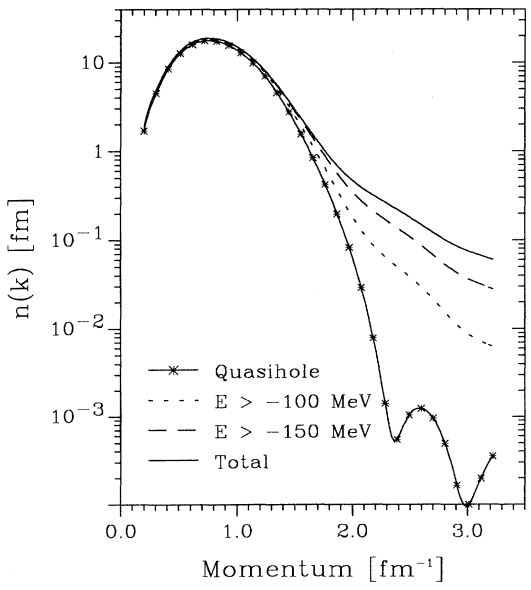

FIG. 6. The total momentum distribution of ^{16}O. Shown are also the quasihole contribution and the results obtained with various energy cutoffs in the integration of the spectral functions.

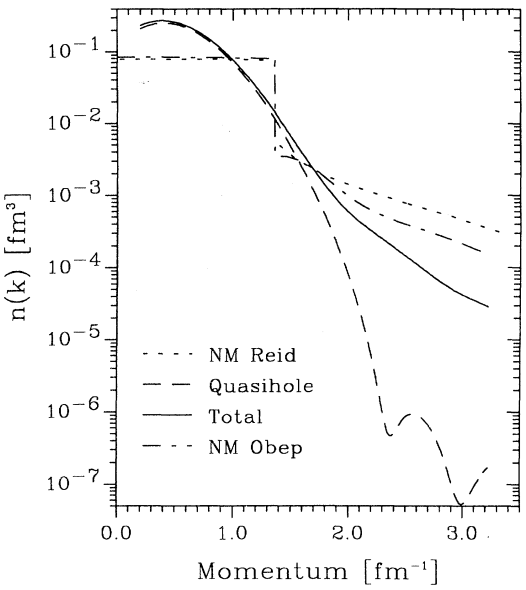

FIG. 7. The total momentum distribution obtained in the present investigation for ^{16}O employing the OBE potential B of Ref. [24] is compared to the momentum distribution obtained in nuclear matter. Also given are results for the Reid soft-core potential in nuclear matter [14]. In this figure the momentum distributions are normalized in such a way that $\int d^3k\, n(k)$ yields 1.

"softer" than the older Reid potential. This is reflected by the fact that the momentum distribution obtained for the Reid potential yields larger values than those obtained for the OBE potential. The comparison between nuclear matter and finite nuclei demonstrates that the enhancement of the momentum distribution predicted by the present study for high momenta is well below the corresponding prediction derived from nuclear matter.

At first sight this discrepancy seems to be in contradiction to the success of the local density approximation found in Ref. [20]. Before we reach this conclusion, however, one must consider the following points: (i) The momentum distributions of nuclear matter have been evaluated for the empirical saturation density. In order to compare with a momentum distribution of a light nucleus, like ^{16}O, the momentum distribution of nuclear matter at around half the saturation density would be more appropriate. The momentum distribution of nuclear matter tends to be smaller at high-momentum transfers for smaller densities [40]. (ii) In our present study of finite nuclei we only consider contributions to the self-energy of the nucleons up to second order in the G matrix (see Fig. 1), whereas the study in nuclear matter accounts for a self-consistent treatment of all ladder diagrams. It is possible that a perturbative approach underestimates the high-momentum components in the distribution, since the G matrix is soft as compared to the bare potential. (iii) Our present approach underestimates the effect of low-energy excitations [see discussion of the single-particle spectrum in calculating the self-energy following Eq. (9)]. For a finite nucleus it is

quite possible that an enhancement of these correlations due to low-energy excitations will provide an enhancement of the momentum distribution around $k = 3$ fm^{-1}. (iv) Finally, we would like to recall that partial waves with $l > 3$, which were ignored in the present study may provide a non-negligible contribution to the momentum distribution at high momenta (see also Fig. 5).

Finally, we would like to discuss the effects of correlations which are taken into account in the present investigation beyond the BHF approximation, on the ground-state properties of ^{16}O. For that purpose Table II lists the ingredients for calculating the total energy of the ground state according to Eq. (31). Furthermore, we present results obtained for the radius of the nucleon distribution [see Eq. (29)].

As a first approximation we consider the Hartree-Fock (HF) approximation, which means that the self-energy of the nucleons is approximated by Eq. (8). This implies that the occupation probabilities are equal to 1 for the three hole states $s_{1/2}$, $p_{3/2}$, $p_{1/2}$, and 0 otherwise. The resulting binding energy per nucleon (−1.93 MeV) is quite small. We believe that this small binding energy is due to the use of the nuclear matter G matrix calculated at the saturation density, which overestimates the Pauli effects as compared to a BHF calculation directly for ^{16}O.

The treatment of the Pauli operator is improved by adding the 2p1h part [Eq. (10)] minus the correction term of Eq. (11) to the self-energy, an approximation which we will call Brueckner-Hartree-Fock (BHF) in the following. Note that the occupation probabilities of the BHF approach are identical to those of the HF approach. Indeed, this correction increases the calculated binding energy to −4.01 MeV. This number is in reasonable agreement with self-consistent BHF calculations performed for ^{16}O using the same interaction [26]. However, as the single-particle states of BHF calculations are more bound than the single-particle states obtained in HF calculations, the gain in the binding energy from HF to BHF calculations is accompanied by a reduction of the calculated radius of the nucleon distribution. This is the well-known phenomenon of the so-called "Coester band" in finite nuclei [26], which plagues microscopic attempts to calculate ground-state properties of nuclear systems already for a very long time [41].

The inclusion of the 2h1p contributions to the self-energy in the complete calculation reduces the absolute values of the quasihole energies (compare BHF and "Total" in Table II). This is to be expected from our discussion following Eq. (12). Despite this reduction of the quasihole energies, however, the total binding energy is increased as compared to BHF calculations. This increase of the binding energy is mainly due to the continuum part of the spectral function. Comparing the various parts of the "Koltun sum rule" of Eq. (31) one finds that only 37% of the total energy is due to the quasihole part of Eq. (31). The dominating part (63%) results from the continuum part of the spectral functions although this continuum part only "represents 11% of the nucleons" (see Table I).

The calculation of the radius, however, is dominated by the quasihole contribution to the density. As the quasihole terms have reduced energies as compared to BHF calculations, it is plausible that the calculated radius in-

TABLE II. Ground-state properties of ^{16}O. Listed are the energies ϵ and kinetic energies t of the quasihole states (qh) and the corresponding mean values for the continuum contribution (c), normalized to 1, for the various partial waves. Multiplying the sum $1/2(t+\epsilon)$ of these mean values with the corresponding particle numbers of Table I, one obtains the contribution ΔE to the energy of the ground state [see the Koltun sum rule Eq. (31)]. Summing up all these contributions and dividing by the nucleon number yields the energy per nucleon E/A. Furthermore, we give the radius for nucleon distribution $\langle r \rangle$, calculated from the square root of Eq. (29). Results are presented for the Hartree-Fock (HF), Brueckner-Hartree-Fock (BHF), and the complete calculation (Total). The particle numbers for the qh states in HF and BHF are equal to the degeneracy of the states; all other occupation numbers are zero. The results for the radii are given in fm, all other entries in MeV.

	HF			BHF			Total		
lj	ϵ	t	ΔE	ϵ	t	ΔE	ϵ	t	ΔE
$s_{1/2}$ qh	-36.91	11.77	-50.28	-42.56	11.91	-61.30	-34.30	11.23	-35.98
$s_{1/2}$ c							-90.36	17.09	-22.89
$p_{3/2}$ qh	-15.35	17.62	9.08	-20.34	18.95	-5.59	-17.90	18.06	0.37
$p_{3/2}$ c							-95.19	35.19	-9.96
$p_{1/2}$ qh	-11.46	16.63	10.34	-17.07	18.46	2.76	-14.14	17.19	5.47
$p_{1/2}$ c							-103.62	35.94	-5.84
$l > 1$ c							-98.87	63.17	-12.27
E/A		-1.93			-4.01			-5.12	
$\langle r \rangle$		2.59			2.49			2.55	

creases in the total calculation as compared to BHF calculations. Therefore the inclusion of 2h1p terms increases the calculated binding energy and radius, moving the results for the ground state off the Coester band into the direction of the experimental data. This effect is large enough to explain the discrepancy obtained between the experimental data and the results of microscopic Dirac-Brueckner-Hartree-Fock calculations for finite nuclei including relativistic effects [42–45]. We note that inclusion of three-body forces in variational calculations for ^{16}O also yields very good results for the binding energy [22].

IV. CONCLUSIONS

An attempt has been made to derive the spectral function and the momentum distribution from a realistic OBE interaction directly for a finite nucleus without the assumption of a local density approximation. The correlations taken into account beyond the Hartree-Fock approximation yield a strong enhancement of the momentum distribution at high momenta. It is demonstrated that this enhancement originates from the spectral function at large negative energies and therefore should be observed in nucleon knockout reactions with large energy transfer leaving the final nucleus at an excitation energy of about 100 MeV.

The enhancement of the high-momentum components is weaker as obtained in studies of nuclear matter. This difference may be due to approximations used in the calculation for the finite system. Therefore further studies of these approximations (poor treatment of low-energy excitations, the self-energy of the nucleons is calculated in a perturbative way including terms up to second order in G) is required before conclusions about the validity of the local density approximation relating the results of nuclear matter to those of finite nuclei can be drawn. Investigations along these lines are in progress.

The resulting Green function is also used to determine the total energy and the radius of the nucleon distribution. It is demonstrated that the inclusion of two-hole–one-particle contributions to the self-energy of the nucleon yields an enhancement of the calculated binding energy per nucleon ($\approx$ 1 MeV) and an increase of the radius ($\approx$ 0.05 fm) for ^{16}O as compared to the Brueckner-Hartree-Fock approach. This could be sufficient to explain the discrepancy remaining between experimental data and microscopic Dirac-BHF calculations for finite nuclei [42–45].

ACKNOWLEDGMENTS

This research project has partially been supported by SFB 382 of the "Deutsche Forschungsgemeinschaft," DGICYT, PB92/0761 (Spain), EC Contract No. CHRX-CT93-0323, and the U.S. NSF under Grant No. PHY-9307484. One of us (H.M.) is pleased to acknowledge the warm hospitality at the Facultad de Fisica, Universitad de Barcelona, and the support by the program for Visiting Professors of this university.

[1] V.R. Pandharipande and R.B. Wiringa, Rev. Mod. Phys. **51**, 821 (1979).
[2] E. Feenberg, *Theory of Quantum Fluids* (Academic Press, New York, 1969).
[3] H. Kümmel, K.H. Lührmann, and J.G. Zabolitzky, Phys. Rep. **36**, 1 (1978).
[4] B.D. Day, Rev. Mod. Phys. **39**, 719 (1967).
[5] W.H. Dickhoff and H. Müther, Rep. Prog. Phys. **55**, 1947 (1992).
[6] H. Morita and T. Suzuki, Prog. Theor. Phys. **86**, 671 (1991).
[7] S. Tadokoro, T. Katyama, Y. Akaishi, and H. Tanaka, Prog. Theor. Phys. **78**, 732 (1987).
[8] C. Ciofi degli Atti, E. Pace, and G. Salmè, Phys. Lett. **141B**, 14 (1984).
[9] O. Benhar and V.R. Pandharipande, Phys. Rev. C **47**, 2218 (1993).
[10] C. Mahaux and R. Sartor, Adv. Nucl. Phys. **20**, 1 (1991).
[11] A. Ramos, A. Polls, and W.H. Dickhoff, Nucl. Phys. **A503**, 1 (1989).
[12] O. Benhar, A. Fabrocini, and S. Fantoni, Nucl. Phys. **A505**, 267 (1989).
[13] C. Ciofi degli Atti, S. Simula, L.L. Frankfurt, and M.I. Strikman, Phys. Rev. C **44**, R7 (1991).
[14] B.E. Vonderfecht, W.H. Dickhoff, A. Polls, and A. Ramos, Nucl. Phys. **A555**, 1 (1993).
[15] C.C. Gearhart, W.H. Dickhoff, A. Polls, and A. Ramos (unpublished).
[16] M. Baldo, I. Bombaci, G. Giansiracusa, U. Lombardo, C. Mahaux, and R. Sartor, Phys. Rev. C **41**, 1748 (1990).
[17] H.S. Köhler, Nucl. Phys. **A537**, 64 (1992).
[18] S. Stringari, M. Traini, and O. Bohigas, Nucl. Phys. **A516**, 33 (1990).
[19] I. Sick, A. Fantoni, A. Fabrocini, and O. Benhar, Phys. Lett. B **323**, 267 (1994).
[20] O. Benhar, A. Fabrocini, S. Fantoni, and I. Sick, Nucl. Phys. **A579**, 493 (1994).
[21] D. Van Neck, A.E.L. Dieperink, and E. Moya de Guerra, report (nucl-th@xxx.lanl.gov:9410019), 1994.
[22] S.C. Pieper, R.B. Wiringa, and V.R. Pandharipande, Phys. Rev. C **46**, 1741 (1992).
[23] S.C. Pieper, in Proceedings of the "6th Workshop on Perspectives in Nuclear Physics at Intermediate Energies," Trieste, 1993 (unpublished).
[24] R. Machleidt, Adv. Nucl. Phys. **19**, 1 (1989).
[25] M. Borromeo, D. Bonatsos, H. Müther, and A. Polls, Nucl. Phys. **A539**, 189 (1992).
[26] K.W. Schmid, H. Müther, and R. Machleidt, Nucl. Phys. **A530**, 14 (1991).
[27] H. Müther and W.H. Dickhoff, Phys. Rev. C **49**, R17

(1994).
[28] D. Bonatsos and H. Müther, Nucl. Phys. **A496**, 23 (1989).
[29] C.W. Wong and D.M. Clement, Nucl. Phys. **A183**, 210 (1972).
[30] M.G.E. Brand, G.A. Rijsdijk, F.A. Muller, K. Allaart, and W.H. Dickhoff, Nucl. Phys. **A531**, 253 (1991).
[31] G.A. Rijsdijk, K. Allaart, and W.H. Dickhoff, Nucl. Phys. **A550**, 159 (1992).
[32] H. Müther and L.D. Skouras, Phys. Lett. B **306**, 306 (1993).
[33] H. Müther and L.D. Skouras, Nucl. Phys. **A581**, 247 (1995).
[34] C. Mahaux, P.F. Bortignon, R.A. Broglia, and C.H. Dasso, Phys. Rep. **120**, 1 (1985).
[35] A. Polls, A. Ramos, H. Müther, C. Gearhart, and W.H. Dickhoff, Prog. Part. Nucl. Phys. (to be published).
[36] W.H. Dickhoff, P.P. Domitrovich, A. Polls, and A. Ramos, in *Condensed Matter Theories*, edited by V.C. Aguilera-Navarro (Plenum, New York, 1990), Vol. 5, p. 275; P.P. Domitrovich, Ph.D. thesis, Washington University, 1991.
[37] J. Mougey, Nucl. Phys. **A335**, 35 (1980).
[38] M. Leuschner *et al.*, Phys. Rev. C **49**, 955 (1994).
[39] H. Müther, A. Polls, and G. Knehr (unpublished).
[40] R.B. Wiringa, V. Fiks, and A. Fabrocini, Phys. Rev. C **38**, 1010 (1988).
[41] F. Coester, S. Cohen, B.D. Day, and C.M. Vincent, Phys. Rev. C **1**, 769 (1970).
[42] R. Fritz and H. Müther, Phys. Rev. C **49**, 633 (1994).
[43] R. Brockmann and H. Toki, Phys. Rev. Lett. **68**, 3408 (1992).
[44] A. Bouyssy, J.-F. Mathiot, Nguyen van Giai, and S. Marcos, Phys. Rev. C **36**, 380 (1987).
[45] F. Boersma and R. Malfliet, Phys. Rev. C **49**, 1495 (1994).